J Mater Sci (2011) 46:3632–3638
DOI 10.1007/s10853-011-5279-0

The influence of deposition temperature on the microstructure of isotropic pyrocarbon obtained by hot-wall chemical vapor deposition

Dong-sheng Zhang · Ke-zhi Li · He-jun Li · Ling-jun Guo · Jin-hua Lu

Received: 26 November 2010 / Accepted: 12 January 2011 / Published online: 26 January 2011

Abstract Bulk isotropic pyrocarbon was successfully prepared by hot-wall chemical vapor deposition. The density of the products was measured by Archimedes method in ethanol. The structural parameters of pyrocarbon were derived from X-ray diffraction (XRD) and Raman spectroscopy. The morphology and texture of pyrocarbon was characterized by scanning electron microscope (SEM) and transmission electron microscope (TEM). The results show that the density of pyrocarbon increases from 1.53 to 1.73 g/cm^3 with the increase of deposition temperature. The d_{002} spacing decreases gradually from 0.3487 to 0.3449 nm as temperature rises from 950 to 1100 °C. Lc increases greatly from 6.5 to 10.5 nm, whereas La slightly rises from 4.0 to 3.6 nm. Under TEM, the fringe lattice images are composed of curved graphene layers, and the length of graphene layers is greatly improved with the increasing temperature. The selected area electron diffraction patterns of the products are complete rings, indicating their isotropic feature.

Introduction

Chemical vapor deposition in hot-wall reactor is the mainly used process to infiltrate porous carbon preforms or to deposit bulk pyrocarbon on various substrates. The chemical vapor deposition of pyrocarbon is influenced by the competitive homogeneous gas phase and heterogeneous surface reactions [1]. Therefore, the overall kinetics of pyrocarbon deposition process is controlled by the competition between homogeneous gas phase and heterogeneous surface reactions [2].

The critical parameters dominating the deposition of pyrocarbon are clearly defined and they are precursor gas, temperature and pressure of pyrolysis, residence time, and the geometry of the reactor (ratio of the surface area of the substrate to the free volume of the precursor gas) [3]. The effect of temperature on pyrocarbon deposition has been studied systemically. It is reported that (1) the deposition rate is correlated with the textures, i.e., increasing deposition rate corresponds to high texture [4]; (2) increasing temperature leads to a strong increasing deposition rate, decreasing partial pressure of ethane and increasing partial pressure of ethene, ethine, and benzene [5]; and (3) the texture improves from low texture to high texture and then deteriorates to low texture again with the increase of temperature [6].

In view of the complexity of chemical vapor deposition process, deposition parameters (temperature, pressure, gas phase composition, the ratio of surface area of substrate to free reaction volume) jointly affect the microstructure and property of the final product. In the present paper, keeping other deposition parameters constant, the effect of temperature on microstructure/texture and crystal parameters of isotropic pyrocarbon (interlayer distance, stack height, and lateral extension) was investigated.

Experiment

Deposition apparatus

The deposition process was carried out in a hot-wall reactor. The experiment equipment is schematically displayed in

D. Zhang (✉) · K. Li · H. Li · L. Guo · J. Lu
The State Key Laboratory of Solidification Processing, Northwestern Polytechnical University, 127, Youyi Road, Xi'an 710072, Shaanxi, People's Republic of China
e-mail: ccnwpu@163.com

Fig. 1. The total length of the reactor is 156 mm. The deposition chamber, made from 40 mm long high purity graphite tube with 52 mm inner diameter and 62 mm outer diameter, was placed at the center of the reactor. A 30-mm-long high purity graphite tube with 32 mm inner diameter and 42 mm outer diameter acting as substrate was fixed in the deposition chamber by a conical shape supporter. The narrow inlet tube with 10 mm inner diameter benefited increasing velocity of gas flow and reducing the predecomposition of the precursor, and the relative wide outlet tube with 25 mm inner diameter was favorable for exhaust emission. The deposition temperature was 950, 1000, 1050, and 1100 °C, and the deposition duration was 20 h. Natural gas with methane purity of 98% was used as carbon source, and diluted by argon with purity of 99.999%. The flow rates of natural gas and argon were separately controlled at 80 and 150 L/h. Natural gas and argon were mixed in mixing chamber and then introduced into deposition chamber. The thickness of the final product was about 5 mm.

Sample characterization

The product was divided into three equal parts along its axial direction (bottom, middle, and top), and the top part was carefully treated for data collection and analysis. The density of pyrocarbon specimens was measured by the Archimedes method in ethanol. X-ray diffraction analysis (X'pert Pro XRD, Copper target with wave length of 0.1541 nm) of rectangular pyrocarbon specimens (10 × 10 × 2 mm) was performed and the original diffraction profiles were corrected with Voigt function. The d_{002} spacing and the apparent stack height (Lc) of the pyrocarbon were derived from the 2θ of (002) peak and full width at half maximum (FWHM) of (002) peak. Renishaw inVia plus Raman spectroscopy with a 514 nm Ar ion laser source was applied to characterize specimens. Raman analysis was performed by single spot using a 50× objective lens. The morphology and texture of the pyrocarbon was observed by scanning electron microscope (SEM JOEL JSM-6460) and transmission electron microscope (TEM JOEL JEM-3010). Morphology analysis was performed on fracture surfaces, and fine powder was scraped off from bulk pyrocarbon products for TEM observation.

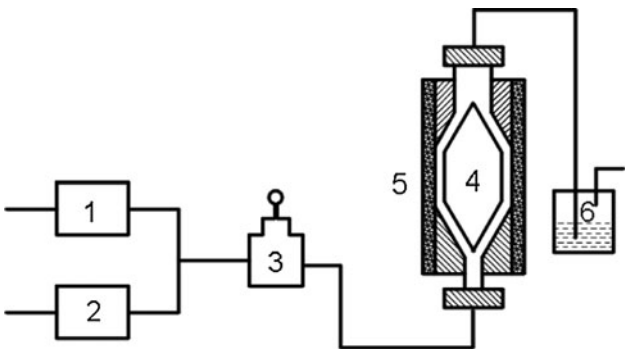

Fig. 1 The scheme of the deposition system, *1* natural gas, *2* argon, *3* mixing chamber, *4* deposition substrate, *5* deposition chamber, and *6* cold trap

Simulation of homogeneous gas phase reactions

The chemical vapor deposition system was not equipped with gas chromatography instrument, to better understand the effect of temperature on the methane pyrolysis, so the homogeneous gas reactions starting from methane were simulated with assistance of CHEMKIN package based on the reported reaction pathways and kinetics of methane decomposition.

Results

Density

The density of the specimens as a function of deposition temperature is shown in Fig. 2. It clearly shows that the density of pyrocarbon gradually rises from 1.53 to 1.73 g/cm^3 with the increasing deposition temperature.

X-ray diffraction

Figure 3 is the XRD profile of the four specimens obtained at different deposition temperatures. The 2θ of (002) peak, FWHM of (002) peak, d_{002} spacing and Lc calculated according to Scherrer equation are all listed in Table 1. The d_{002} spacing of the specimens slowly declines from 0.3487

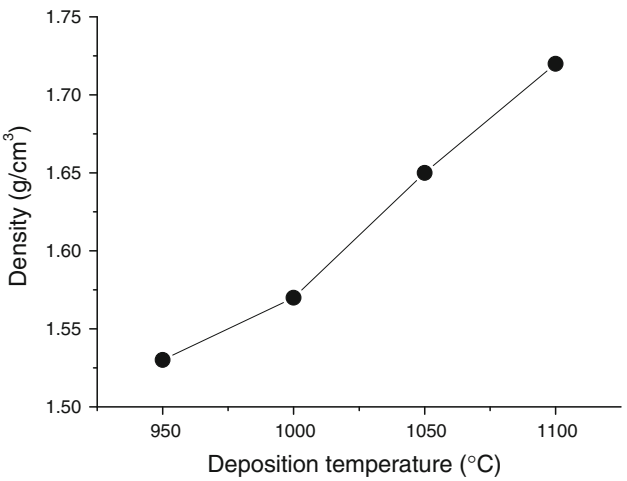

Fig. 2 The density of the four specimens obtained by the Archimedes method as a function of deposition temperature

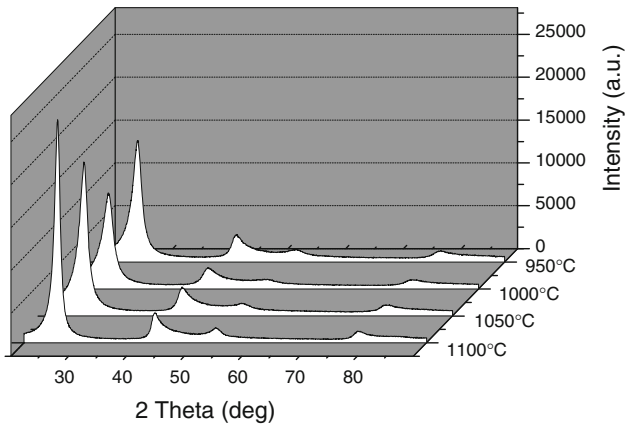

Fig. 3 XRD profiles of the pyrocarbon samples obtained at different temperatures

Table 1 XRD results of the pyrocarbon samples obtained at different temperatures

	2θ (°)	FWHM of (002) peak (°)	d_{002} spacing (nm)	Lc (nm)
950 °C	25.53	2.73	0.3487	6.2
1000 °C	25.75	2.64	0.3457	6.5
1050 °C	25.78	2.01	0.3454	8.5
1100 °C	25.82	1.62	0.3449	10.5

to 0.3449 nm with the increase of deposition temperature, while the Lc increases from 6.5 to 10.5 nm. These clearly indicate that increasing deposition temperature is beneficial to improve the crystalline of pyrocarbon.

Scanning electron microscopy

The morphology of fracture surface of the specimens obtained at different deposition temperatures is shown in Fig. 4. In Fig. 4a, pyrocarbon obtained at low deposition temperature (950 °C) is constituted by irregular globular structure loosely compacted together, and the size of the pores in Fig. 4a is relatively big. The globular structure are gradually weakened and the roughness of the globules are markedly decreased (Fig. 4b–d) with the increasing deposition temperature. In addition, the diminishing pores with the increase of deposition temperature are responsible for the upward tendency of density of the four specimens.

Transmission electron microscopy

The texture of pyrocarbon is analyzed by TEM and the terminology utilized to describe pyrocarbon texture is the one proposed by Reznik and Hüttinger [7] on the basis of preferred orientation of fundamental structural units. According to the differences in orientation angle obtained from azimuthal intensity scans of SAED patterns [8], four kinds of pyrocarbon texture are quantitatively defined as high texture, medium texture, low texture, and isotropic.

Figure 5 shows the fringe lattice images of the four specimens obtained at different temperatures. In general, the graphene fringe length and its curvature gradually increase with the increase of deposition temperature. In Fig. 5a, the short graphene fringe merely has short-range order and orients randomly. The graphene fringe length is evidently increased, and its orientation is improved to a great extent (Fig. 5b). In Fig. 5c and d, the length and height of graphene fringe is increasingly improved with the deposition temperature increasing. The selected area diffraction patterns inserted in Fig. 5a–d are a complete ring, which demonstrates their isotropic characterization.

Raman spectroscopy

The Raman spectrum of the four specimens in Fig. 6 shows two first order lines locating at about 1350 cm^{-1} (D band) and 1588 cm^{-1} (G band) and two second-order lines locating at about 2700 and 2900 cm^{-1}. The first-order lines are correlated to the intralayer disorder, while the second-order lines are believed to relate to structural changes along the c axis [9–11]. The growing intensity of D band indicates the increase of in-plane disorder in the graphic structure, and the reducing intensity at full width at half maximum (FWHM) reveals the improvement of graphitization. Furthermore, the ratio of the D band intensity to that of G band is frequently used to empirically calculate the in-plane crystallite size La with the following equation [12, 13]:

$$\mathrm{La}\ (\mathrm{nm}) = 4.4\,(I_\mathrm{D}/I_\mathrm{G})^{-1} \quad (1)$$

In Fig. 6, with the increase of deposition temperature, the D band slightly decreases, whereas the FWHM of the G band increases. All these indicate the in-plane disorder reduces, while the graphitization is significantly promoted with the increase of deposition temperature, which is consistent with the results originating from XRD and TEM. In-plane crystallite size, La, calculated from Eq. 1 is plotted in Fig. 7. La slimly changing from 3.6 to 4.0 nm is obtained as the deposition temperature varies from 950 to 1100 °C. These conspicuously suggest that raising deposition temperature improves crystallite size of pyrocarbon.

Discussion

The effect of temperature on pyrocarbon formation

The formation mechanism of pyrocarbon involving with the elementary reactions and process of carbon formation is

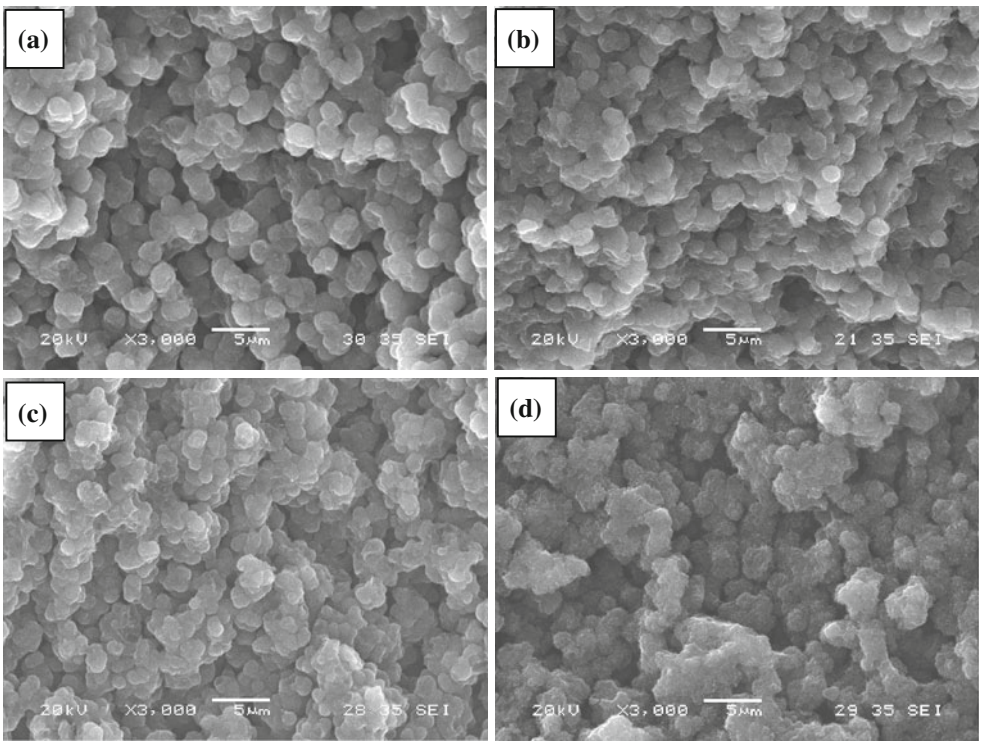

Fig. 4 The fracture surface morphology of the four specimens obtained at different temperature: **a** 950 °C, **b** 1000 °C, **c** 1050 °C, **d** 1100 °C, respectively

directly related to pyrocarbon texture, which ranged from isotropic to low, medium, and high texture [7].

According to the elementary reactions of methane pyrolysis [14–18], the relationship between the deposition temperature and the gas phase reactions was simulated using CHEMKIN package under the assumption that mixture gas flew in plug flow pattern in deposition chamber. The simulation results are shown in Fig. 8.

Resulting from its low reaction constant at low deposition temperature, only less than 2% methane was pyrolyzed (950 and 1000 °C). As the deposition temperature rise, more and more methane molecules were involved in pyrolysis reactions. Hydrogen as the main byproduct was in low quantity at 950 and 1000 °C. At 1100 °C, the yield of hydrogen sharply increased. Ethane and ethene as the primary products of methane pyrolysis were the predominant intermediates, which would play an important role in the formation of pyrocarbon. Benzene, the primary aromatic hydrocarbons, began to emerge at 1050 °C, and its yield was greatly raised at 1100 °C.

The effect of temperature on the deposition of pyrocarbon

Starting from the nucleation and the growth processes on a given substrate, the heterogeneous surface reactions were the decisive step controlling the rate of pyrocarbon deposition [19]. For chemical vapor deposition in hot-wall reactors, the ratio of the area of the substrate surface to the free reaction volume (A_S/V_R) was a decisive parameter. For a large surface area of the substrate, heterogeneous surface reactions were favored and a large amount of reactive intermediates were removed from the gas phase. For a high reactor volume, a great amount of reactive species probably were in a low fraction [20]. The A_S/V_R value of deposition chamber in these experiments was relative low, about 0.18 mm^{-1}. This low A_S/V_R value would theoretically favor homogeneous gas phase reactions and reactive intermediates with heavy molecular weight should be formed. However, ethane and ethene were the main components according to the simulation results. This disparity between the theoretical and simulation results may be ascribed to the relatively short residence time. The precursor gas in deposition chamber was renewed in short residence time and the formation of intermediates with heavy molecular weight was badly inhibited.

Associated with adsorption and desorption on the surfaces of substrate, these heterogeneous surface reactions remained challenges, though many studies had been carried out to better understand these intrinsic mechanisms [21–25]. A detailed chemical route from ethane to benzene and to pyrocarbon was qualitatively proposed to explain these experimental data.

According to the simulation results, to form pyrocarbon, these small linear hydrocarbons, ethane and ethene, had to

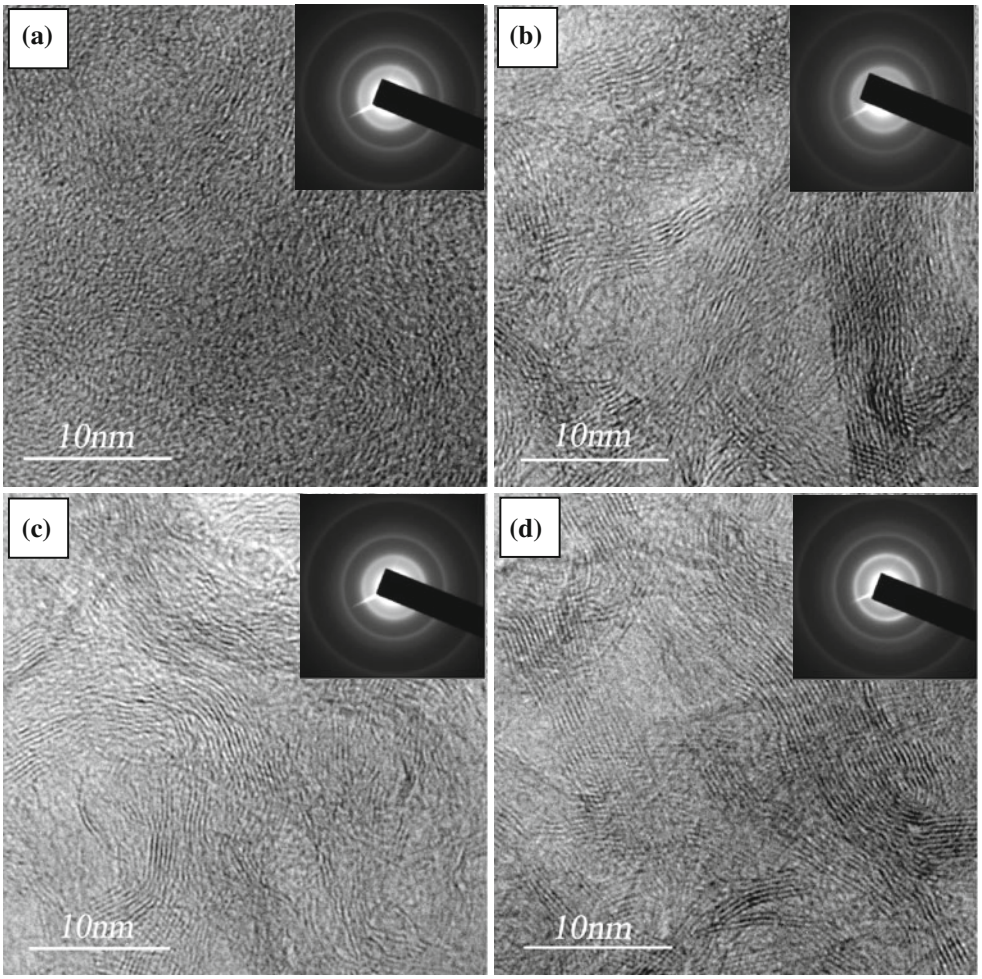

Fig. 5 Transmission electron microscope of pyrocarbon obtained at different deposition temperature: **a** 950 °C, **b** 1000 °C, **c** 1050 °C, **d** 1100 °C. The SAED patterns of pyrocarbon are inserted in **a**, **b**, **c**, and **d**, respectively

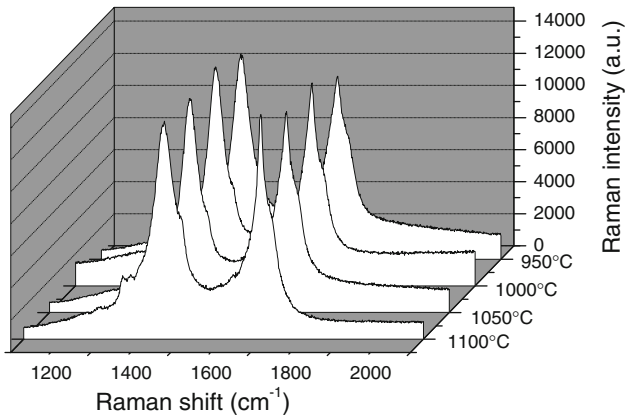

Fig. 6 The Raman spectrum of the four specimens as function of deposition temperature

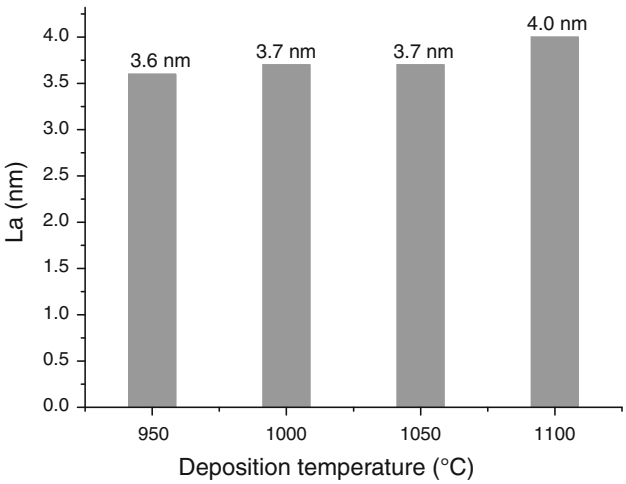

Fig. 7 La values plotted against deposition temperature

transfer to six-membered ring network as the basic structural unit through a series of intermediate states. The overall procedure was shown in Fig. 9. For ethene, its molecules firstly were activated through continuous collision with other molecules in gas phase and dissociated into vinyl and hydrogen before they were chemisorbed onto the active sites locating at the surface of substrate. The

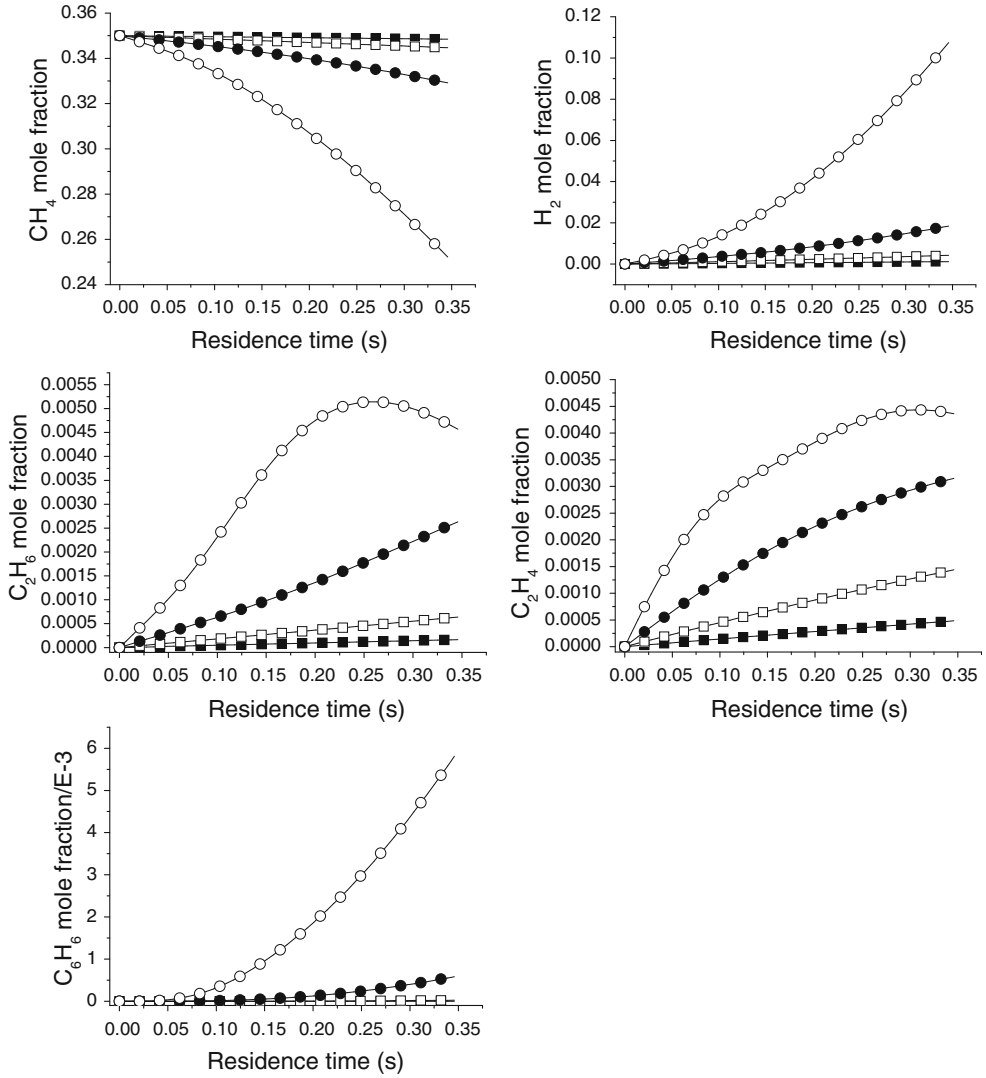

Fig. 8 Gas compositions analyses as a function of residence time obtained at constant deposition temperature. *Filled square* 950 °C, *open square* 1000 °C, *filled circle* 1050 °C, *open circle* 1100 °C

chemisorbed vinyl was subsequently collided by molecules coming from gas phase to form N-C_4H_5. At last, six-membered ring was produced via successive vinyl addition reaction. For ethane, it initially had to be di-σ-hybridized to form ethene, and the following reaction pathway for ethane was the same with that of ethene.

At 950 °C, ethane and ethene on one hand contributed to the further growth of basic structural unit and on the other hand to the formation of new growth sites. However, their low fraction limited the expansion of basic structural unit along *a*, *b*, and *c* direction. That was why the value of Lc and La were small (Table 1; Fig. 7) and the length of graphene layers were short (Fig. 5a). With the increase of deposition temperature, the mole fraction of ethane and ethene were slowly increased, and consequently, the value of Lc and La were accordingly raised to 6.5 and 3.7 nm (Table 1, Fig. 7). The length of graphene layers were markedly prolonged (Fig. 5b). At 1050 °C, benzene started to show its influence on pyrocarbon deposition and formation. The Lc value sharply increased from 6.5 to 8.5 nm. But benzene played a significant role in the improvement of Lc and La at 1100 °C. The value of Lc and La reached to 10.5 and 4.0 nm. With the increase of ethane, ethene, and benzene, the densification of pyrocarbon was slightly promoted and the pores were slowly eliminated. But the size of the pyrocarbon particles did not change remarkably, and this may be attributed to the predominant role of ethane and ethene (Fig. 8).

Conclusions

In the present paper, the influence of deposition temperature on the microstructure of isotropic pyrocarbon was studied. According to the above discussion, the following

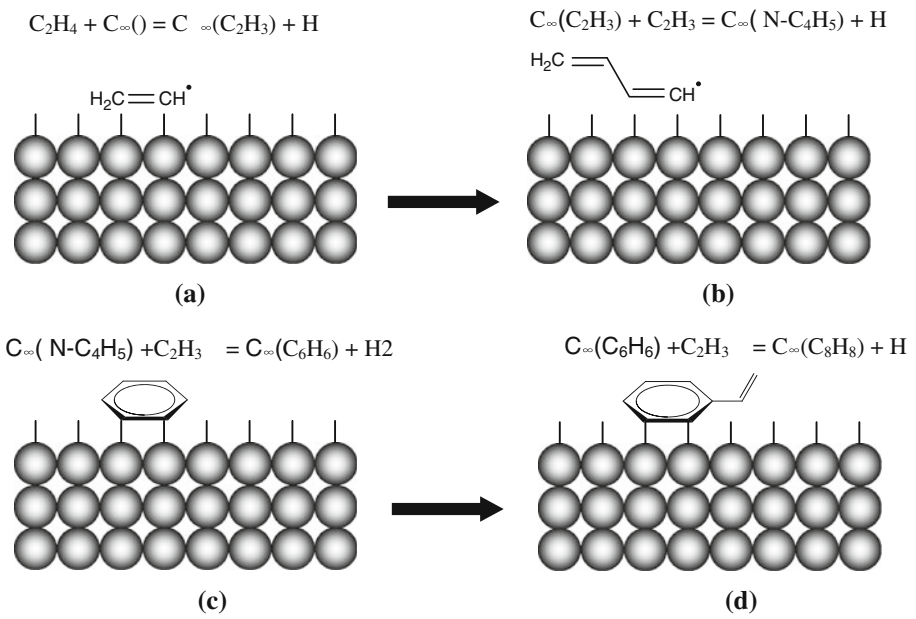

Fig. 9 The overall surface reaction process of ethene

conclusions could be drawn for isotropic pyrocarbon at 950–1100 °C.

(1) With methane as the main carbon source, homogeneous reactions in the gas phase are dominated by formation of small linear hydrocarbon species.
(2) With the increase of deposition temperature, the density of isotropic pyrocarbon increases from 1.53 to 1.73 g/cm^3.
(3) The crystalline of isotropic pyrocarbon is markedly improved, i.e. Lc is increased from 6.5 to 10.5 nm, and La is raised from 3.6 to 4.0 nm.
(4) The length of graphene layer is remarkably increased.

Acknowledgement The research is financially supported by the Natural Science Foundation of China under Grant Nos. 50832004 and 50972120, and the Program of Introducing Talents of Discipline to University under Grant No. B08040.

References

1. Hüttinger KJ (1998) Chem Vap Deposition 4:151
2. Norinaga K, Deutschmann O, Huttinger KJ (2006) Carbon 44:1790
3. Oberlin A (2002) Carbon 40:7
4. Pauw VD, Kalhöfer S, Gerthsen D (2004) Carbon 42:279
5. Brüggert M, Hu Z, Hüttinger KJ (1999) Carbon 37:2021
6. Hu ZJ, Zhang WG, Hüttinger KJ, Reznik B, Gerthsen D (2003) Carbon 41:749
7. Reznik B, Hüttinger KJ (2002) Carbon 40:621
8. Bourrat X, Trouvat B, Limousin G, Vignoles G (2000) J Mater Res 15:92
9. Yoshida A, Kaburagi Y, Hishiyama Y (2006) Carbon 44:2333
10. Dillon RO, Woolen JA (1984) Phys Rev B 29:3482
11. Honorato EL, Meadows PJ, Shatwell RA, Xiao P (2010) Carbon 48:881
12. Tuinstra F, Koening JL (1970) J Chem Phys 53:1126
13. Knight D, White WB (1989) J Mater Res 4:385
14. Benzinger W, Becker A, Hüttinger KJ (1996) Carbon 34:957
15. Becker A, Hüttinger KJ (1998) Carbon 36:177
16. Li HJ, Li AJ, Bai RC, Li KZ (2005) Carbon 43:2937
17. Norinaga K, Deutschmann O (2007) Ind Eng Chem Res 46:3547
18. Glasier GF, Pacey PD (2001) Carbon 39:15
19. Delhaes P (2002) Carbon 40:641
20. Teubner M, Hu ZJ, Hüttinger KJ (2000) High Temp High Pressures 32:725
21. Quli FA, Thrower PA, Radovic LR (1998) Carbon 36:1623
22. Pfrang A, Wan YZ, Schimmel T (2010) Carbon 48:921
23. Li KZ, Zhang DS, Guo LJ, Li HJ (2010) J Mater Sci Technol 26:1133
24. Kim Mh, Lee KY (1987) J Mater Sci 22:3988. doi:10.1007/BF01133348
25. Je JH, Lee JY (1985) J Mater Sci 20:839. doi:10.1007/BF00585724